RSC Advances

PAPER

View Article Online
View Journal | View Issue

Check for updates

Cite this: *RSC Adv.*, 2025, **15**, 13431

Synthesis and application of idesia oil-based imidazoline derivative as an effective corrosion inhibitor for Q235 steel in hydrochloric acid medium†

Zhen Hu, [a] Fen Yi[b] and Hailian Yu*[a]

Idesia oil-based imidazoline derivative (IOID) as a corrosion inhibitor was synthesized through the solvent dehydration method for Q235 steel in HCl solution. It was characterized by FTIR, and the corrosion inhibition performance was evaluated by static weight loss testing and electrochemical measurements. The corrosion inhibition mechanism of IOID was also investigated. The results indicated that the optimized synthetic method for IOID involved a 1 : 1 molar ratio of imidazoline intermediate to quaternization reagent, under a quaternization reaction temperature of 80 °C and a quaternization reaction time of 2 h. The inhibition efficiency of over 99.07% was achievable when 40 ppm IOID was applied in 1 M HCl solution at 80 °C, even after the inhibitor was used for one week. The corrosion inhibition mechanism involved the corrosion products covering the steel substrate surface and forming a dense protective film. Physical adsorption occurred on the steel substrate surface, which played a protective role for Q235 steel.

Received 31st December 2024
Accepted 24th February 2025

DOI: 10.1039/d4ra09103e

rsc.li/rsc-advances

Open Access Article. Published on 28 April 2025. Downloaded on 6/13/2026 3:19:14 AM.
This article is licensed under a Creative Commons Attribution-NonCommercial 3.0 Unported Licence.

1. Introduction

The global issue of acid corrosion in the field of gas/oil transportation through pipelines has attracted significant concern for decades.[1–3] Acidic gas and liquid remaining in deacidification devices can cause severe corrosion to pipelines, threatening the surrounding ecosystem through exhaust leaks.[4,5] The chemical production processes that involve acid leaching, descaling, and boiler descaling are carried out under acidic conditions, which also lead to severe corrosion of equipment at a higher rate than in other media.[6–8] In addition, approximately 2% to 4% of global gross domestic product is lost due to corrosion hazards, according to statistics, which is higher than the annual economic losses caused by floods and fires.[9,10] Furthermore, about 10% to 20% of annual steel production worldwide is lost due to corrosion, resulting in an economic loss of 3 billion dollars per year.[11] Therefore, to address the technical problems related to corrosion, significant capital and efforts are invested, leading to increased operating costs for enterprises.[12,13] To tackle this issue, research on corrosion inhibitors applied to acidic media is essential, offering effective and low-cost approaches to mitigate corrosion and prevent severe damage.[14] Among many organic corrosion inhibitors, imidazoline corrosion inhibitors have attracted widespread attention due to their low toxicity, environmental friendliness and green characteristics.[15,16] Some studies show that the heteroatoms N, O and S in imidazoline and its derivative molecules can form coordination bonds with iron atoms in carbon steel, and the double bonds in molecules can also form π–d bonds with metal, enhancing their adsorption capacity and forming a protective film on the metal surface that prevents the corrosive medium from contacting the metal.[17–19] Among these corrosion inhibitors, imidazoline corrosion inhibitors play an important role in protecting metals from corrosion. These imidazoline intermediates are positively charged under acidic conditions and exhibit good water solubility, especially at high temperatures.[20,21] Conventionally, imidazoline corrosion inhibitors are synthesized using raw materials such as lauric acid, oleic acid and coconut oleic acid. However, there are few reports on the synthesis of imidazoline from natural idesia oil. Idesia oil contains rich fatty acids with conjugated double bonds, making it a preferred source for synthesizing imidazoline derivatives.[22–26] Additionally, idesia oil has the characteristics of renewability, low cost, easy availability and is environmentally friendly. In this study, a two-step method was used to synthesize an imidazoline quaternary ammonium salt corrosion inhibitor using idesia oil as the raw material. The corrosion inhibition performance was evaluated using polarization curves and electrochemical impedance spectroscopy. The surface morphology of Q235 carbon steel was also analyzed, and its corrosion inhibition mechanism was studied by XPS, providing a new approach for imidazoline quaternary ammonium salt corrosion inhibitors.

[a]*School of Chemical Engineering, Sichuan University of Science & Engineering, Sichuan, P. R. China. E-mail: yhl19791027@126.com*

[b]*Sichuan Vocational College of Chemical Technology, Sichuan, P. R. China*

† Electronic supplementary information (ESI) available. See DOI: https://doi.org/10.1039/d4ra09103e

© 2025 The Author(s). Published by the Royal Society of Chemistry

Open Access Article. Published on 28 April 2025. Downloaded on 6/13/2026 3:19:14 AM. This article is licensed under a Creative Commons Attribution-NonCommercial 3.0 Unported Licence.

2. Experimental

2.1 Reagents and materials

Experiments were carried out using Q235 carbon steel as the specimen with the following composition (in wt%): C, 0.16%; Mn, 0.53%; Si, 0.30%; P, 0.045%; S, 0.055%; Ni, 0.3%; Cu, 0.3%; and Fe, 98.31%. Idesia oil was purchased, and other analytical grade raw materials including xylene, diethylenetriamine, phenylboronic acid, bromothymol, petroleum ether and absolute ethanol were purchased commercially. The corrosive medium solution was prepared by diluting HCl (analytical grade, 37%) with distilled water.

2.2 Experimental methods

2.2.1 Synthesis of IOID

(1) Amidation reaction. Idesia oil (27.66 g) and xylene (10.00 mL) as the water-carrying agent were added into a 250 mL three-necked flask, followed by the addition of 4 g of zeolite to prevent bumping. After the reaction system was heated to 433.15 K, the organic amine reagent was slowly added to the above three-necked flask through a constant pressure funnel; the reaction mixture was then heated to 140 °C and refluxed for 3 h until no water droplet was generated in the water separator.

(2) Cyclization reaction. The reaction mixture was further heated to 200 °C to remove vapour and refluxed until no water droplet was produced in the water separator.

(3) Quaternization reaction. When the above reaction mixture was cooled to 70 °C, quaternary amine reagent was slowly added through a constant pressure dropping funnel, and a reddish-brown and translucent viscous liquid product formed, which was the imidazoline quaternary ammonium salt corrosion inhibitor.

2.3 Product analysis methods

2.3.1 Infrared spectroscopy of IOID. The synthesized organic corrosion inhibitor and its intermediate were characterized by a Nicolet 6700 FTIR spectrometer (Thermo Fisher Scientific) within the working range of 400–4000 cm^{-1}. The sample preparation process was carried out under a tungsten lamp drying condition, the corrosion inhibitor and intermediate were mixed with the dried potassium bromide crystal powder in a ratio of 100 : 1 respectively, and the mixed powder was flattened into a transparent film with a thickness of 1 mm and diameter of 10 mm by the KBr pressing method in a mold. Its infrared spectrum was analyzed by a FTIR spectrometer.

2.3.2 Component analysis of IOID. The components of IOID were determined by bromothymol blue spectrophotometry within 400–700 nm.

2.4 Performance evaluation of IOID

2.4.1 Water solubility of IOID. Water solubility of inhibitor in corrosive medium solution was measured by adding a certain amount of IOID to the 1 M HCl corrosive medium. The corrosive medium solution was shaken and left at ambient temperature for 24 h. The ambient temperature was maintained by using a constant temperature water bath during water solubility measurements. The clarity, turbidity and precipitation of the solution was recorded accordingly.

2.4.2 Weight loss measurements. The experiments were performed using Q235 carbon steel specimens with a size of 4 cm × 1.3 cm × 0.2 cm, which were abraded with a series of emery papers (grade 320, 500, 800 and 1200). IOID was added to 500 mL HCl corrosive medium and soaked for 24 h. After the corrosion experiments were finished, the carbon steel test sheets were ultrasonically cleaned, then washed with acetone and distilled water. The corrosion rate (R) and inhibition efficiency (IE%) were calculated using the following equations:

$$R = w/s \times t$$

$$\mathrm{IE\%} = [(R_0 - R)/R_0] \times 100\%$$

where w is the average weight loss of three parallel carbon steel sheets, s is the total area of the specimens, t is immersion time, and R_0 and R are the values of the corrosion rate without and with addition of inhibitor, respectively.

2.4.3 Electrochemical measurements. (1) Electrochemical impedance spectroscopy measurements: electrochemical tests were carried out using an electrochemistry workstation. The sample was embedded in epoxy resin with an exposed area of 1 cm^2 employed as working electrode. The exposed surface of the embedded sample was abraded successively with 100 to 1200 grade SiC papers.

(2) EIS measurements and polarization curves were carried out in a typical three-electrode setup in the frequency range of 100 kHz to 10 mHz using a perturbation of 10 mV amplitude at the open circuit potential (E_{ocp}) under an atmospheric pressure using a three-electrode jacketed test cell with a working volume of 250 mL used as a container. This three-electrode consisted of a saturated calomel electrode (SCE) (reference electrode (RE)), a 1 cm^2 Pt plate (auxiliary electrode (CE)) and a 10 mm × 10 mm × 30 mm Q235 specimen (working electrode (WE)). The WE with a 1 cm^2 exposed surface was treated before electrochemical experiments by abrading with emery paper from 100 to 1200 grade, then rinsing gently with adequate distilled water and washing with absolute ethyl alcohol. Polarization studies were performed at ±400 mV *vs.* SCE at OCP at a scan rate of 0.5 mV s^{-1}, the corrosion current density value was calculated using Tafel extrapolation, and each test was repeated three times to ensure the accuracy of the result.

2.4.4 Surface characterization. The morphologies and composition of the Q235 steel specimens formed on the steel surface were investigated using a scanning electron microscope and X-ray photoelectron spectrometer.

The morphologies of the Q235 steel specimens after corrosion were observed using a JSM-7500F field emission scanning electron microscope (SEM, Japan Electron Optics Laboratory Co. Ltd). Before observation, the Q235 steel specimens were rinsed ultrasonically with ethyl alcohol. The SEM was analyzed at an accelerating voltage of 20 kV and the micrographs of the Q235 steel specimens were obtained at different magnifications. The composition and chemical states of the Q235 steel

© 2025 The Author(s). Published by the Royal Society of Chemistry

Open Access Article. Published on 28 April 2025. Downloaded on 6/13/2026 3:19:14 AM. This article is licensed under a Creative Commons Attribution-NonCommercial 3.0 Unported Licence.

specimens were analyzed using XSAM800 X-ray photoelectron spectroscopy (Axis Ultra XPS, Kratos Analytical, UK), using Mg Kα radiation (1486.6 eV) with the pass energy of 50 eV, beam spot diameter of 3 mm, and power set to 300 W.

3. Results and discussion

3.1 FTIR analysis of IOID and its intermediate

3.1.1 FTIR analysis of intermediate of IOID. The structural characteristic of synthesized intermediate was confirmed by FTIR spectroscopy between 400–4000^{-1} cm.

As shown in Fig. 1, the peak at 3409 cm^{-1} is identified as the N–H stretching vibrational peak on the aromatic ring, the peaks at 2922 cm^{-1} and 2875 cm^{-1} belong to C–H stretching vibrational peaks of –CH_2– and –CH_3–, respectively, the peak at 1625 cm^{-1} is the C=N stretching vibrational peak on the ring, and the peaks at 715 cm^{-1} and 1067 cm^{-1} belong to characteristic peaks of N–H and five-membered aromatic rings, respectively. These peaks indicate that the product contains a five-membered heterocyclic imidazoline ring structure, confirming that the product is the intermediate of imidazoline quaternary ammonium salt.

3.1.2 FTIR analysis of IOID. The structural characteristic of synthesized inhibitor is confirmed by FTIR spectroscopy in the range of 4000–400^{-1} cm.

The FTIR spectrum of IOID (Fig. 2) is similar to the IR spectrum of imidazoline intermediate (Fig. 1). The peak at 3402 cm^{-1} is the N–H stretching vibrational peak on the ring, while peaks at 2934 cm^{-1} and 2849 cm^{-1} belong to the C–H stretching vibrational peaks of –CH_2– and –CH_3–, respectively, the peak at 1612 cm^{-1} is the C=N stretching vibrational peak on the ring, the peaks at 778 cm^{-1} and 1048 cm^{-1} belong to characteristic peaks of N–H and five-membered aromatic rings, respectively, and these peaks are assigned to characteristic peaks of imidazoline. The peaks at 1454 cm^{-1} and 1368 cm^{-1} are the characteristic peaks of the C–N bond and C=P bond on the imidazoline ring, and the peak at 2359 cm^{-1} is the characteristic peak of C–PO_3–N. These peaks are the characteristic peaks of Idesia oil based imidazoline derivative, which is an indication of the successful synthesis of the desired IOID.

3.2 Corrosion inhibition performance and weight loss studies of IOID

3.2.1 Water solubility evaluation of IOID. The water solubility of inhibitor was measured and the water solubility of corrosion inhibitor with different mass fractions at different temperatures was also investigated. The experimental results are shown in Table 1.

It can be seen from Table 1 that the temperature has no obvious effect on water solubility, the quaternized imidazoline inhibitor has improving water solubility at increasing concentration, and the solution system is relatively stable, which indicates that the synthesized inhibitor has good water solubility and thermal stability.[27]

3.2.2 Effect of inhibitor concentration on inhibition performance. Inhibitor concentrations of 10, 20, 30, 40, 50, 60, and 70 ppm were added to 1 M HCl medium solution at 30 °C, and their inhibition effect on carbon steel was measured after incubation in the corrosive medium for 24 h. The effect of inhibitor concentration on its inhibition performance is shown in Fig. 3.

It can be seen from Fig. 3 that the inhibitor has a good inhibition effect in the HCl medium, even at a lower concentration (such as 20 ppm). The inhibition rate gradually increases and then stabilizes with the continuous increase in the inhibitor concentration. When the concentration of the inhibitor continues to increase, the inhibitory effect of inhibitor also increases, which indicates that the inhibitor has a positive effect

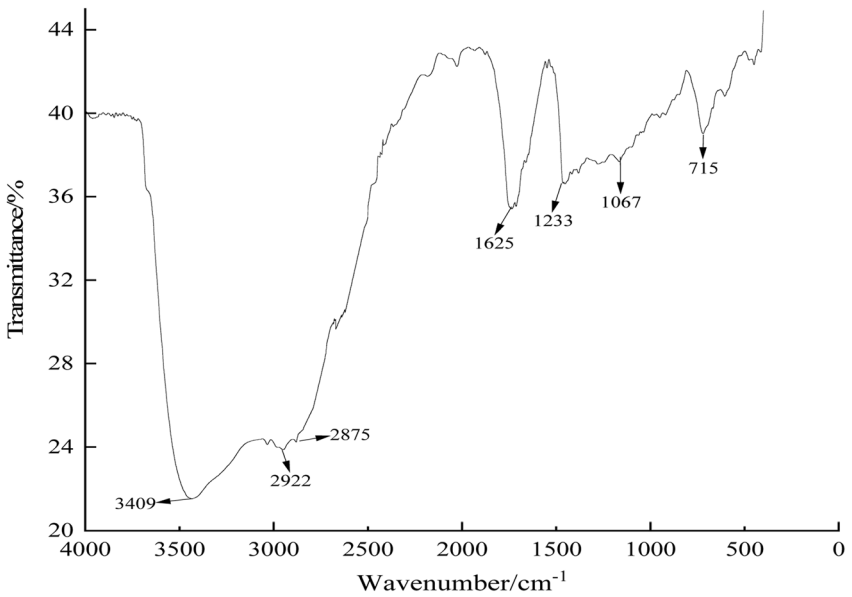

Fig. 1 FTIR of intermediate of IOID.

Open Access Article. Published on 28 April 2025. Downloaded on 6/13/2026 3:19:14 AM. This article is licensed under a Creative Commons Attribution-NonCommercial 3.0 Unported Licence.

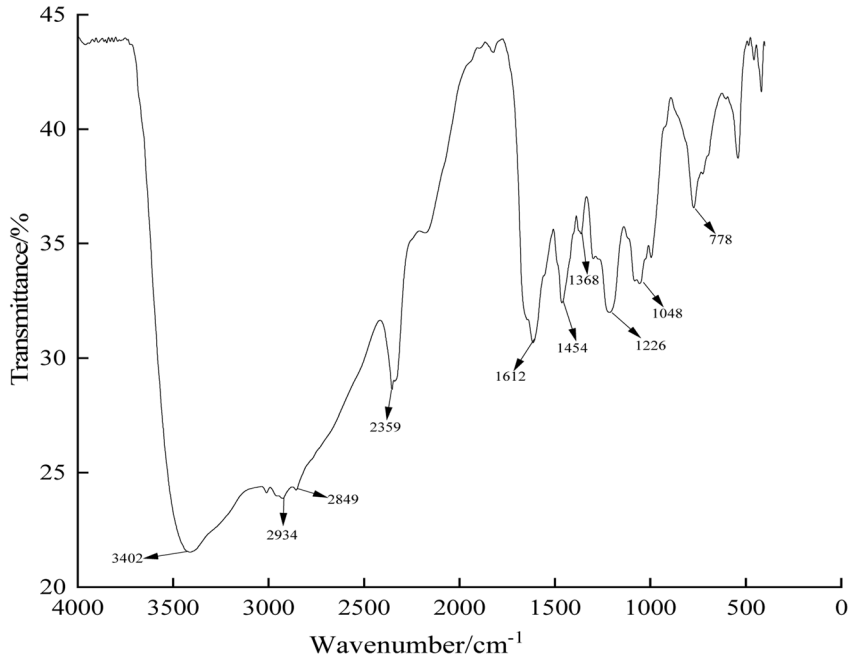

Fig. 2 FTIR of IOID.

Table 1 Water solubility of IOID

Mass fraction of IOID/%	Temperature/°C					
	10	20	30	40	50	60
10%	Soluble	Soluble	Soluble	Soluble	Soluble	Soluble
15%	Soluble	Soluble	Soluble	Soluble	Soluble	Soluble
30%	Soluble	Soluble	Soluble	Soluble	Soluble	Soluble
40%	Soluble	Soluble	Soluble	Soluble	Soluble	Soluble

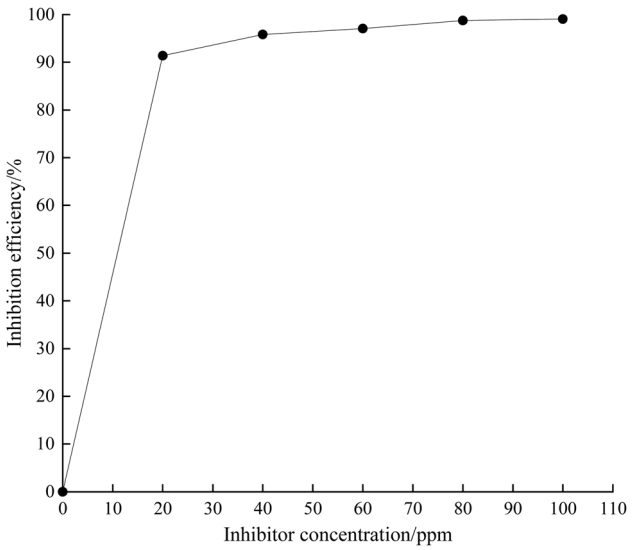

Fig. 3 Effect of IOID concentration on the inhibition of carbon steel in HCl solution.

on the adsorption layer that protects the metal surface.[28] When the concentration of inhibitor was 40 ppm, the inhibition efficiency reached 95%, and the corrosion inhibition effect is better than that in ref. 11.

3.2.3 Effect of corrosion time on inhibition performance. At 30 °C, the inhibitor concentration was 40 ppm. After carbon steel was corroded in a 1 M HCl solution for 1–7 days, the inhibition effect of IOID on carbon steel was investigated. The experimental results are shown in Fig. 4.

The inhibition efficiency is the highest when the carbon steel is corroded for 1 day in the HCl medium solution (Fig. 4). However, the inhibition rate gradually decreases with the increase of corrosion time. Because IOID is an adsorption film inhibitor, the formed protective film partially falls off from carbon steel substrate with the extension of corrosion time.[29] As a result, the imidazoline quaternary ammonium salt inhibitor covering the surface of carbon steel decreases, which reduces the inhibition rate. However, the inhibition rate is still higher than 94.2% in the HCl medium solution after 4 d.

3.2.4 Effect of corrosion inhibition temperature on inhibition performance. The inhibitor concentration was 40 ppm, and carbon steel was corroded in a 1 M HCl solution for 24 h at different temperatures. The effect of inhibition temperature on carbon steel was investigated, and the experimental result is shown in Fig. 5.

It can be seen from Fig. 5 that when the inhibition temperature is below 80 °C, the inhibition rate is above 90%, indicating that the corrosion inhibitor exhibits better corrosion inhibition effects at temperatures below 80 °C. However, once the inhibition temperature exceeds 80 °C, the inhibition rate decreases significantly, suggesting that the inhibition is greatly restricted at temperatures above 80 °C. When the corrosion inhibition

© 2025 The Author(s). Published by the Royal Society of Chemistry

Open Access Article. Published on 28 April 2025. Downloaded on 6/13/2026 3:19:14 AM.
This article is licensed under a Creative Commons Attribution-NonCommercial 3.0 Unported Licence.

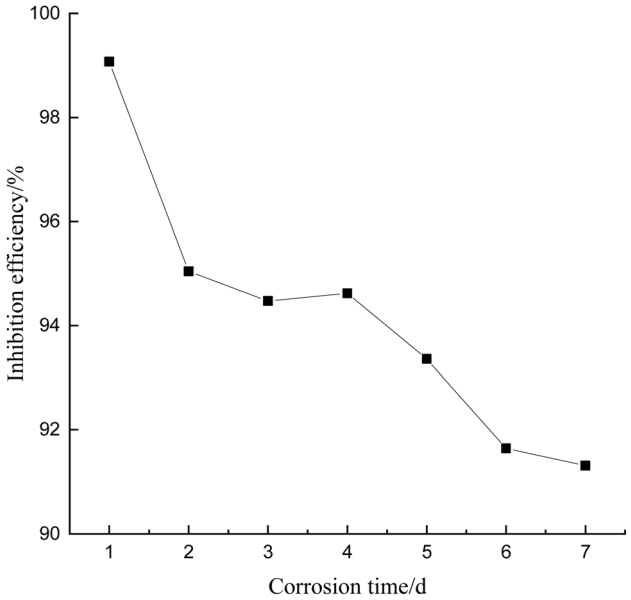

Fig. 4 Effect of corrosion time on the inhibition of carbon steel in HCl solution.

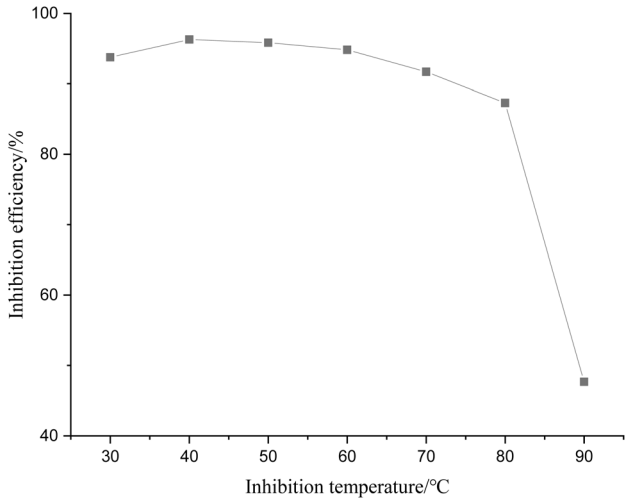

Fig. 5 Effect of inhibition temperature on corrosion inhibition of carbon steel in HCl medium solution.

temperature is below 40 °C, the inhibition rate continues to increase. This is because the quaternary ammonium salt imidazoline inhibitor is an adsorption film inhibitor and the molecular motion rate is low at low temperature, with the inhibitor having less opportunity to form coordination bonds with the metal substrate, and the inhibition rate is higher than that of the metal surface. When the inhibition temperature rises, the probability of forming coordination bond increases with increasing molecule motion, and the number of inhibitors adsorbing on the metal surface increases, favoring the formation of a layer on the film, so the inhibition rate gradually increases.[30] The molecule motion rate continues to increase at an inhibition temperature higher than 40 °C. Coordination bonds are easily broken if the molecule motion rate reaches a higher level. Hence, the formed protective film is partially damaged, the inhibition rate decreases, and the inhibitor will desorb from the formed adsorption film.

3.3 Electrochemical studies

3.3.1 Polarization curve analysis. Fig. 6 shows the potentiodynamic polarization curves for carbon steel with different concentration of inhibitor measured *via* electrochemical tests.

Adding inhibitor to the HCl corrosion medium solution has negative effects on the cathodic reaction and anodic dissolution of carbon steel (Fig. 6). The polarization curve tends to move to the lower left with increasing inhibitor concentration, and the self-corrosion potential moves significantly to more negative, but the shift in amplitude is less than 85 mV. Therefore, this inhibitor should be categorized as a cathodic type inhibitor. This finding shows that protection from aggressive solution may significantly influence the coverage rate of corrosion inhibition molecules on carbon steel surface. The inhibition efficiencies calculated from the polarization tests present the same trend as those obtained from the weight loss measurements. The shape of potentiodynamic polarization curves in the inhibited solutions significantly changed with respect to those in the blank solution, suggesting that the corrosion process on steel surface was deeply affected by corrosion inhibitor.

The electrochemical parameters such as corrosion potential (E_{corr}), corrosion current density (I_{corr}) and other parameters with inhibition efficiency are listed in Table 2.

With the increase of inhibitor concentration, the current density decreases gradually. In this case, an effective protective film is formed when inhibitor molecules adsorb on the carbon steel surface, which prevents further corrosion of carbon steel surface by the corrosive medium. This shows that the synthesized inhibitor can effectively inhibit the corrosion of carbon steel in HCl solution.

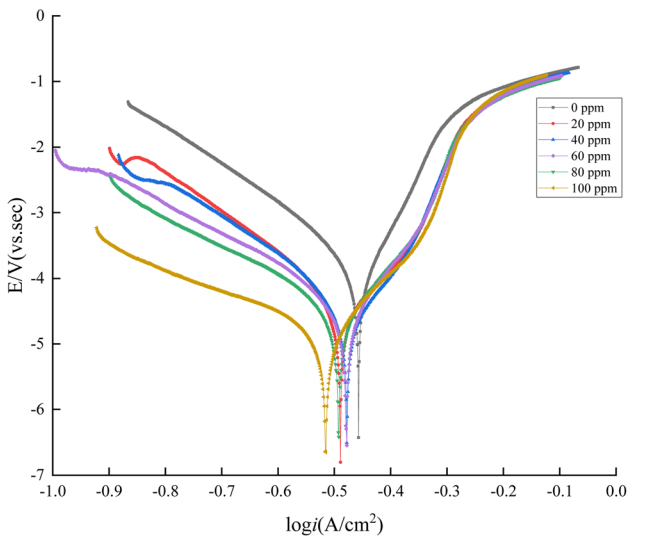

Fig. 6 Polarization curves of carbon steel under different concentrations of corrosion inhibitor in HCl solution.

Open Access Article. Published on 28 April 2025. Downloaded on 6/13/2026 3:19:14 AM. This article is licensed under a Creative Commons Attribution-NonCommercial 3.0 Unported Licence.

Table 2 Electrochemical parameters of polarization curve fitting of IOID in HCl solution

Conc. (ppm)	E_{corr} (mV *vs.* SCE)	I_{corr} (μA cm^{-2})	η_p (%)	R_{ct} (Ω cm^2)	CPE_{dl} (μf cm^{-2})	η_z (%)
Blank	−439.7	87.12	—	144.3	—	—
20	−475.7	17.03	80.45	835.7	146.5	82.73
40	−454.6	11.25	87.09	1072	110	86.54
60	−480	10.14	88.36	1403	106.4	89.71
80	−472	8.46	90.29	1615	105.6	91.06
100	−519.4	7.25	91.68	2009	99.5	92.82

3.3.2 Electrochemical impedance spectroscopy. Fig. 7 shows Nyquist plots and Bode plots for carbon steel in hydrochloric acid solution with different concentrations of IOID.

The Nyquist plot in Fig. 7 contains only a clear semi-circular arc, and there is no obvious second peak in the Bode plot. This indicates that the electrochemical behavior of the system can be fitted to impedance spectra using an equivalent circuit model with a single time constant.[31] Additionally, the radius of the capacitive resistance arc of the Nyquist diagram in the hydrochloric acid solution medium is significantly larger than that in the absence of corrosion inhibitor, indicating that IOID embodies good acidic corrosion inhibition performance.

Since both the Nyquist plot and Bode plot exhibit the characteristic of a single time constant, simple equivalent circuit models can be used to fit the experimental data. The specific parameters of the equivalent circuit can be obtained through fitting and used for further analysis of the performance of corrosion inhibitors. EIS spectra were analyzed using the equivalent circuit in Fig. 8(A) and (B) in 1 M HCl solution in the absence and presence of inhibitor, respectively.

In Fig. 8, R_{ct} is the charge transfer resistance, R_s is the solution resistance, C_{d1} is the constant phase angle element, R_{cp} is the membrane resistance of the product, and C_{cp} is the membrane capacitance of the product. Fig. 8(A) is used to fit the spectrum measured when no corrosion inhibitor is added to the HCl solution medium, where a significant number of corrosion products are deposited on the surface of carbon steel. Fig. 8(B)

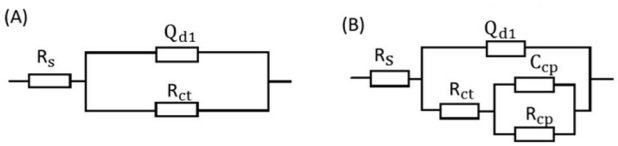

Fig. 8 Equivalent circuit diagram used to fit the impedance spectrum of carbon steel: (A) absence of inhibitor and (B) presence of inhibitor.

is used to fit the spectrum measured when the corrosion inhibitor is added to the HCl solution medium. Compared to Fig. 8(A), it is more suitable for situations where non-ideal capacitance behavior occurs on the electrode surface, such as on rough surfaces or adsorption layers. In addition to the above three components, the equivalent circuit diagram of Fig. 8(B) also contains membrane capacitance of product (C_{cp}) and membrane resistance of product (R_{cp}); therefore, it is suitable for situations where there is an adsorption layer on the electrode surface. The corresponding fitted parameters were presented in Table 3.

3.3.3 Adsorption isotherm analysis. Table 4 shows the measurement results of the corrosion inhibition rate and coverage rate of carbon steel when different concentrations of corrosion inhibitor were added to the HCl solution medium.

The adsorption thermodynamic of corrosion inhibitor was analyzed. After substituting the concentration of corrosion inhibitor and the corresponding coverage rate θ into the

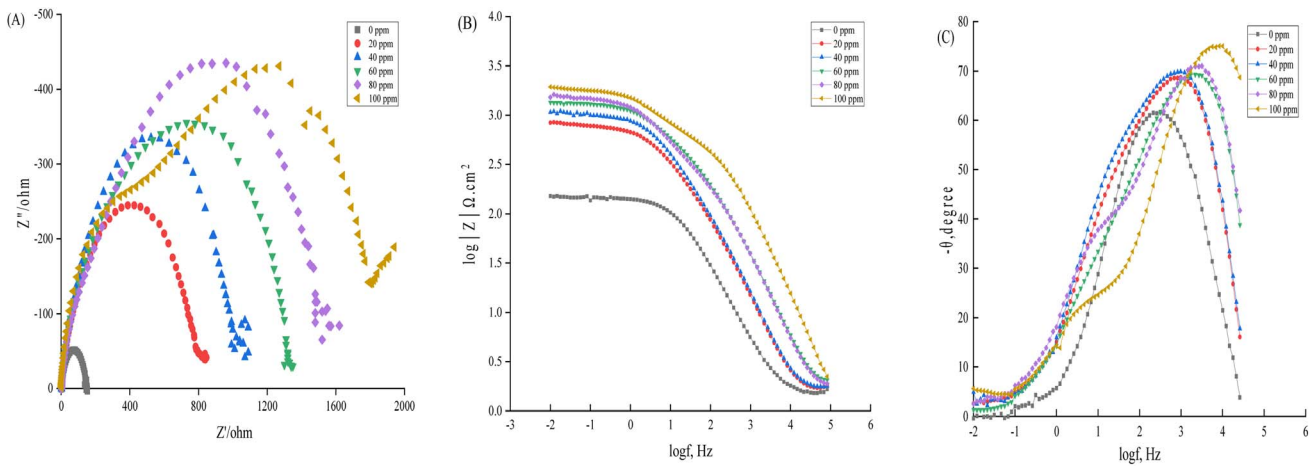

Fig. 7 Nyquist plots (A) and Bode plots (B and C) of carbon steel in hydrochloric acid solution containing different concentrations of IOID (the impedance was normalized by the area).

© 2025 The Author(s). Published by the Royal Society of Chemistry

Open Access Article. Published on 28 April 2025. Downloaded on 6/13/2026 3:19:14 AM. This article is licensed under a Creative Commons Attribution-NonCommercial 3.0 Unported Licence.

Table 3 Fitting results of the EIS curves of corrosion inhibitor in HCl medium

Parameter	Symbol	Unit	Model 1 (R(QR))	Model 2 (R(C(R(QR))))
Solution resistance	R_s	Ω	10.5	10.2
Charge-transfer resistance	R_{ct}	Ω	1500	1450
Constant phase element	Q	S s^n	1.2×10^{-5}	—
CPE index	n	—	0.85	0.8
Double layer capacitance	C_{dl}	F	—	2.5×10^{-6}
Adsorption layer resistance	R_{ads}	Ω	—	200
Adsorption layer capacitance	C_{ads}	F	—	1.0×10^{-7}

Table 4 Corrosion inhibition rate of concentration of corrosion inhibitor in HCl medium

Conc./ppm	W g^{-1}	ν/mg cm^{-1} h^{-1}	η/%	θ/%
0	0.3020	12.0994	0	0
10	0.02647	1.0605	91.23	91.22
20	0.02613	1.0469	91.35	91.34
30	0.0201	0.8053	93.34	93.31
40	0.0096	0.3846	96.82	96.81
50	0.00887	0.3554	97.06	97.04
60	0.0098	0.3926	96.75	96.71
70	0.01033	0.4139	96.58	96.57

adsorption isotherm, the adsorption process of corrosion inhibitor conformed to the Langmuir adsorption isotherm, as shown in the following formula:

$$\frac{C}{\theta} = \frac{1}{K_{ads}} + C$$

where C and K_{ads} are the inhibitor concentration and equilibrium constant, respectively. The standard free energy of adsorption (ΔG^0_{ads}) was calculated using the following equation:

$$\Delta G^0_{ads} = -RT\ln(55.5K_{ads})$$

where 55.5 is the molar concentration of water in the solution expressed in mol units (mol L^{-1}), R is the gas equilibrium constant and temperature T is 303.15 K.

The correlation coefficient (R^2) of C/θ and C of the corrosion inhibitor is close to 1 (Fig. 9). Estimations of K_{ads} and ΔG^0_{ads} according to the above equations indicated that the corrosion inhibitor has stable and uniform adsorption on the surface of carbon steel in hydrochloric acid solution. The adsorption of corrosion inhibitor on the surface of carbon steel in hydrochloric acid solution follows the Langmuir adsorption isotherms with the formation of a layer of film that prevents steel from corrosion by the medium. Conventionally, this adsorption type belongs to chemisorption when ΔG^0_{ads} is greater than 40 kJ mol^{-1} due to the sharing of charges or charge transfer from the inhibitor molecule to the metal surface to form a covalent bond. When ΔG^0_{ads} is lower than 20 kJ mol^{-1}, this adsorption type was considered as physisorption, and the adsorption behavior between metal and inhibitor molecules is mainly driven by electrostatic attraction. When ΔG^0_{ads} is between 20 kJ mol^{-1} and 40 kJ mol^{-1}, the inhibitor adsorption involves both interaction of chemisorption and physisorption.

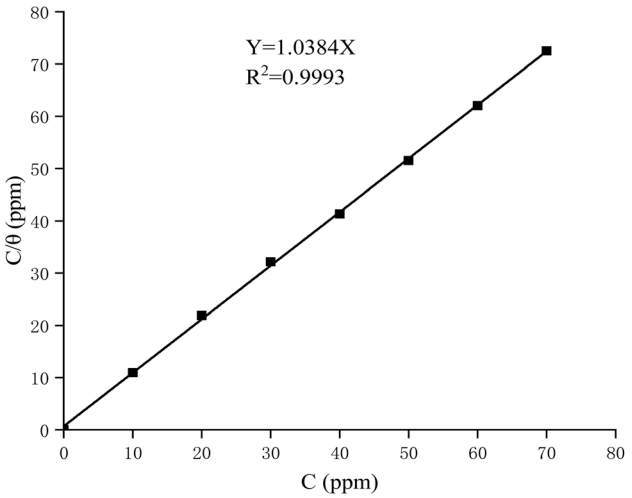

Fig. 9 Relationship between C/θ and C of the corrosion inhibitor in HCl solution.

The corrosion inhibitor molecules can adsorb spontaneously (Table 3). When ΔG^0_{ads} is −41.56 kJ mol^{-1}, the corrosion inhibitor forms a chemical bond and stably adsorbs on the surface of carbon steel through the hydrophilic groups, exhibiting a good protective effect.

3.3.4 SEM analysis of Q235 carbon steel. Fig. 10 shows the morphology of carbon steel surfaces under different conditions. Fig. 10(A) shows surface morphology of original carbon steel uncorroded; Fig. 10(B) shows surface morphology of carbon steel corroded in 1 M HCl solution in the absence of corrosion inhibitor, Fig. 10(C) shows surface morphology of carbon steel corroded in 1 M HCl solution in the presence of corrosion inhibitor whose concentration is 40 ppm.

It can be seen from Fig. 10(A) that the surface of carbon steel is less corroded. From Fig. 10(B), it can be seen that after the carbon steel is immersed in the hydrochloric acid solution without a corrosion inhibitor, some corrosion pits are observed. Moreover, a layer of obvious corrosion product forms on the surface of the carbon steel. While these corrosion products can protect the metal surface from further corrosion to a certain extent, once the partial corrosion products are destroyed, more severe pitting corrosion will occur. In Fig. 10(B), the corrosion degree of the carbon steel surface is not uniform, and the entire carbon steel surface exhibits severe corrosion. In Fig. 10(C), the corrosion of carbon steel is not obvious, the surface of carbon steel is relatively smooth, and there is an adsorption film on the

Open Access Article. Published on 28 April 2025. Downloaded on 6/13/2026 3:19:14 AM. This article is licensed under a Creative Commons Attribution-NonCommercial 3.0 Unported Licence.

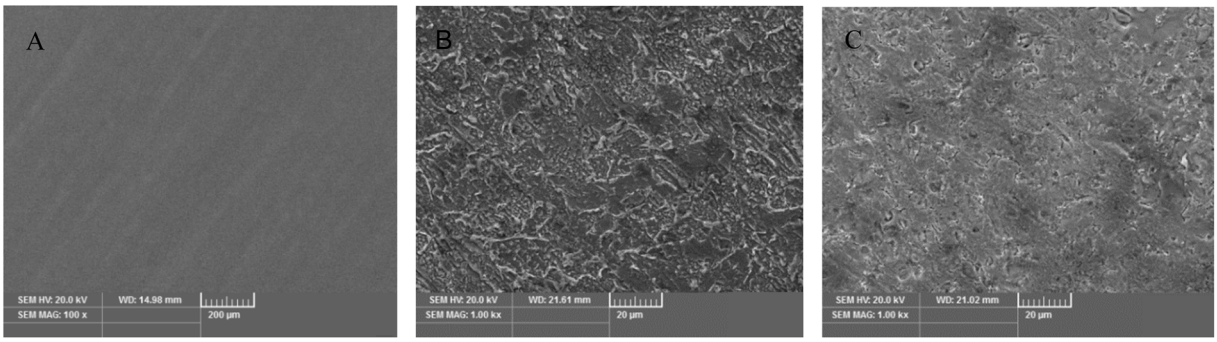

Fig. 10 Scanning electron microscope of carbon steel. (A) The surface of the original uncorroded carbon steel; (B) the surface of carbon steel corroded in 1 M HCl solution without corrosion inhibitor; (C) the surface morphology of carbon steel corroded in 1 M HCl solution with 40 ppm corrosion inhibitor.

surface of carbon steel. Because the corrosion inhibitor molecules adsorb on the surface of carbon steel, it is completely covered by a layer of corrosion inhibitor molecules. This improves the surface smoothness of carbon steel, and hinders the corrosion caused by acidic media.

3.3.5 XPS studies. The high resolution and XPS full spectra obtained for the surface of carbon steel immersed in 1 M hydrochloric acid solution containing 40 ppm of corrosion inhibitor is displayed in Fig. 11.

Surface N, C, O and Fe elements were detected after carbon steel was corroded in HCl solution containing 40 ppm of corrosion inhibitor for 24 h at room temperature.

The high-resolution spectrum of Fe 2p exhibits peaks at 710.20 eV, 713.37 eV and 724.59 eV (Fig. 12). The peak at 710.20 eV is assigned to the characteristic peak of Fe–Cl in the ferric compound, $FeCl_2$, which is attributed to the reaction between hydrochloric acid and carbon steel base. The peak at 713.37 eV is associated with the satellite peak of Fe–Cl in $FeCl_2$, while the peak at 724.59 eV belongs to carbon steel substrate. In the N 1s spectrum, the peak at 399.12 eV is identified as the C═N bond of the C═N–C group, while the peak at 399.77 eV is the C–N bond of the –CH–NH_2 group in the imidazoline quaternary ammonium salt. The results show that the imidazoline quaternary ammonium salt adsorbs on the surface of carbon steel, and an N atom in the imidazoline ring reacts with the empty d orbital in the iron atom to form a stable Fe–N coordination bond. This improves the activation energy of anode reaction in the corrosive medium and the corrosion rate of carbon steel is reduced significantly by the corrosion inhibitor. In the O 1s spectrum, the peak at 529.55 eV belongs to the Fe–O bond of FeO, where Fe base is oxidized, the peak at 531.06 eV corresponds to the P═O– bond of the imidazoline quaternary ammonium salt. In the C 1s spectrum, the peaks at 529.55 eV and 284.80 eV are characteristic peaks of C. The peak at 284.33 eV is consistent with the C–C bond of –CH_2CH_2–, while the peak at 284.80 eV is linked to the C–H bond of –CH_2CH_2–. The surface composition analysis of corroded carbon steel shows that carbon steel reacts with hydrochloric acid to form $FeCl_2$ and oxygen dissolved in the corrosive medium forms FeO. The $FeCl_2$ and FeO corrosion products closely cover the surface of carbon steel to form a dense protective film. On the other hand, one end of the corrosion inhibitor molecule containing the C═N–C group is connected to the iron base, so it closely adsorbs on the surface of iron substrate. The long nonpolar alkyl chain in the corrosion inhibitor molecule is far away from the metal surface and extends to the end of the corrosive solution, forming a layer of hydrophobic film to prevent the corrosive medium from contacting carbon steel. The corrosion inhibitor has a protective effect for the surface of carbon steel, indicating that the inhibitor molecules form a stable adsorption film on the surface, which is consistent with the adsorption thermodynamics results discussed earlier. In addition to physical adsorption, corrosion inhibitor molecules also participate in chemical adsorption, and these two kinds of adsorption behavior synergistically protect the carbon steel surface.

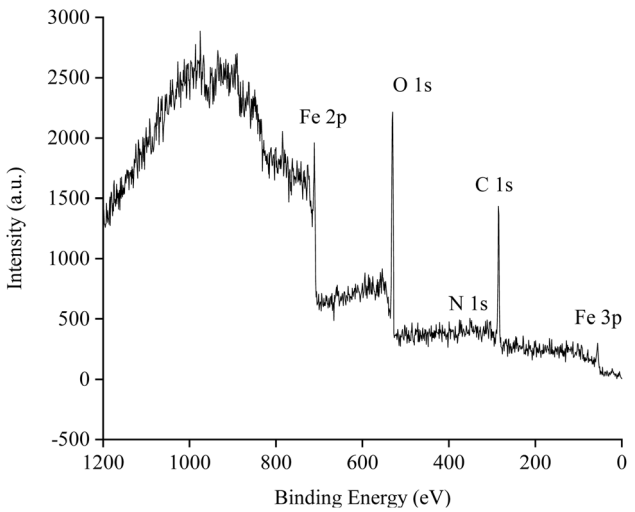

Fig. 11 XPS full spectrum of the carbon steel surface after corrosive treatment using 1 M hydrochloric acid solution containing 40 ppm of corrosion inhibitor.

3.4 Corrosion inhibition mechanism by IOID

The analysis of adsorption thermodynamics shows that the adsorption of corrosion inhibitor on the surface of carbon steel in hydrochloric acid solution meets Langmuir adsorption

© 2025 The Author(s). Published by the Royal Society of Chemistry

Open Access Article. Published on 28 April 2025. Downloaded on 6/13/2026 3:19:14 AM.
This article is licensed under a Creative Commons Attribution-NonCommercial 3.0 Unported Licence.

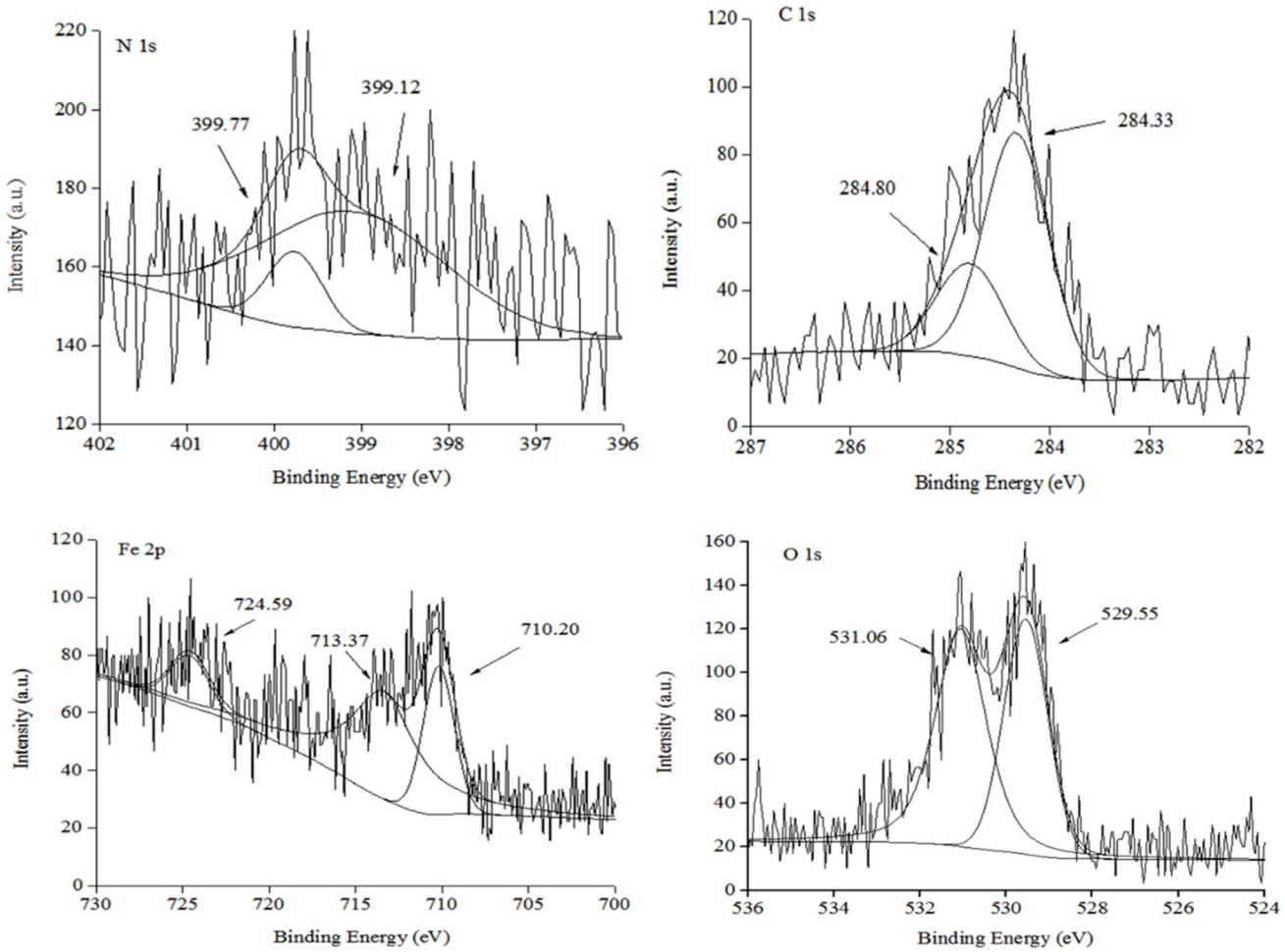

Fig. 12 High-resolution spectra of carbon steel surface after corrosion in 1 M of hydrochloric acid solution containing 40 ppm of corrosion inhibitor.

isotherms, which prevents the steel from corrosion induced by the corrosion medium. The imidazoline quaternary ammonium salt molecules produce chemical adsorption on the surface of carbon steel and the lone pairs of N atom in the inhibitor molecule provide empty d orbital for iron, so that the corrosion inhibitor forms a coordination bond with steel substrate and produces a stable protective film, thereby effectively inhibiting the corrosion to carbon steel. The weight loss method, electrochemical method and scanning electron microscope analysis shows that the corrosion inhibitor adsorbs on the surface of carbon steel in hydrochloric acid solution, which plays a protective role for carbon steel. Carbon steel encountered total corrosion in hydrochloric acid solution, while the inhibitor can adsorb quickly and stably on the surface of carbon steel to form a layer of dense and stable protective film, which has a protective effect. The analysis of XPS shows that carbon steel substrate reacts with hydrochloric acid and produces $FeCl_2$. Fe also reacts with oxygen dissolved in the corrosive medium to form FeO, and these $FeCl_2$ and FeO corrosion products closely attach on the surface of carbon steel, which prevents further corrosion of inner carbon steel. The end of the corrosion inhibitor molecule containing a C=N–C group is connected to the iron substrate, which adsorbs closely on the surface of iron substrate. The long chain alkyl group in the inhibitor molecule is far away from the metal surface and extends to the end of the corrosive solution medium, forming an adsorption film. This protective barrier prevents the corrosive medium from contacting carbon steel, which is conducive to reducing corrosion. Physical adsorption

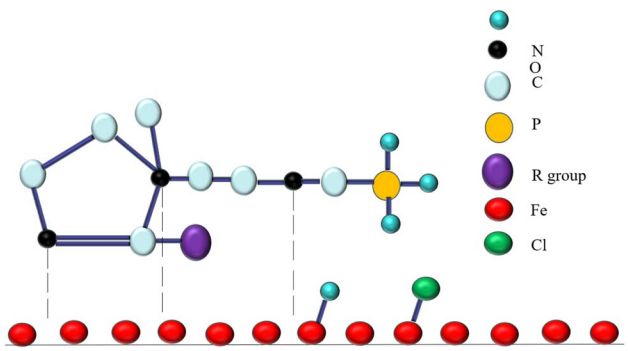

Fig. 13 Schematic illustration of the adsorption mechanism of corrosion inhibitor on the carbon steel surface.

Open Access Article. Published on 28 April 2025. Downloaded on 6/13/2026 3:19:14 AM. This article is licensed under a Creative Commons Attribution-NonCommercial 3.0 Unported Licence.

and chemical adsorption formed by corrosion inhibitor molecules play a synergistic protective role.

More specifically, the interaction between corrosion inhibitor and metal surface is illustrated in Fig. 13.

4. Conclusion

Idesia oil based imidazoline corrosion inhibitor was synthesized by the solvent dehydration method. After optimization, the synthesis process of IOID used a 1 : 1 molar ratio of imidazoline intermediate to quaternization reagent, the quaternization reaction temperature and time was 80 °C and 2 h, respectively, with a desirable water solubility and thermal stability.

The inhibition efficiency reached 99.07% after 40 ppm of IOID was placed in hydrochloric acid solution below 80 °C. The corrosion inhibitor still exhibits excellent corrosion inhibition performance after one week.

The analysis of scanning electron microscopy, the electrochemical method and XPS show that carbon steel substrate reacts with hydrochloric acid and produces $FeCl_2$. During corrosion, carbon steel substrate also reacts with oxygen dissolved in the corrosive medium to form FeO, and these corrosion products closely cover the surface of carbon steel, which prevents further corrosion of the inner layer. The adsorption mode of IOID on the surface of carbon steel belongs to Langmuir isotherm adsorption, with a ΔG^0_{ads} of -41.56 kJ mol^{-1}, and the C═N–C group in the corrosion inhibitor molecule is attached on the surface of iron substrate and prevents corrosive substances to directly contact the surface of carbon steel, which is conducive to protecting carbon steel. The corrosion inhibitor synthesized in this study can be applied to crude oil pipelines to prevent acidic corrosion.

Data availability

The data supporting this article have been included as part of the ESI.†

Conflicts of interest

There are no conflicts to declare.

Acknowledgements

The authors acknowledge the financial supports of the Key Laboratory of Fine Chemicals and Surfactants in Sichuan Provincial Universities (No. 2017JXZ01).

References

1 N. A. Negm, A. M. A. Sabagh, M. A. Migahed, H. M. A. Bary and H. I. Din, Effectiveness of some diquaternary ammonium surfactants as corrosion inhibitors for carbon steel in 0.5 M HCl solution, *Corros. Sci.*, 2010, **52**, 2122–2132.
2 D. M. Ortega-Toledo, J. G. Gonzalez-Rodriguez, M. Casales, M. A. Neri-Florez and A. Martinez-Villafane, The CO_2 corrosion inhibition of a high strength pipeline steel by hydroxyethyl imidazoline, *Mater. Chem. Phys.*, 2010, **122**, 485–490.
3 A. I. Thorhallsson, A. Stefansson, D. Kovalov and S. N. Karlsdottir, Corrosion testing of materials in simulated superheated geothermal environment, *Corros. Sci.*, 2020, **168**, 108584–1085597.
4 X. F. Zhang, T. Ma, X. C. Hua, J. J. Zheng, X. Y. Wang and S. X. Rao, Flow accelerated naphthenic acid corrosion during high acid crude oil refining, *Eng. Failure Anal.*, 2020, **117**, 104802–104816.
5 P. C. Okafor and Y. G. Zheng, Synergistic inhibition behaviour of methylbenzyl quaternary imidazoline derivative and iodide ions on mild steel in H_2SO_4 solutions, *Corros. Sci.*, 2009, **51**, 850–859.
6 D. R. Qu, Y. G. Zheng and H. M. Jing, High temperature naphthenic acid corrosion and sulphidic corrosion of Q235 and 5Cr1/2Mo steels in synthetic refining media, *Corros. Sci.*, 2006, **48**, 1960–1985.
7 J. Zhang, X. L. Gong, H. H. Yu and M. Du, The inhibition mechanism of imidazoline phosphate inhibitor for Q235 steel in hydrochloric acid medium, *Corros. Sci.*, 2011, **53**, 3324–3330.
8 J. Liu, H. F. Li, Y. Zhou, Z. W. Pan and S. X. Rao, Influence law of temperature and turbulence on naphthenic acid corrosion of low carbon steel, *Acta Pet. Sin., Pet. Process. Sect.*, 2016, **32**, 556–563.
9 X. G. Li, D. W. Zhang, Z. Y. Z. Li, C. W. Du and C. F. Dong, Materials science: share corrosion data, *Nature*, 2015, **527**, 441–442.
10 L. Gang, Q. H. Song, X. J. Wang, X. T. Jiang, J. Q. Jin and D. U. Lei, Performance of a kind of self-made imidazoline derivative corrosion inhibitor, *Corros. Prot.*, 2017, **38**, 40–44.
11 L. Zhang, Y. He, Y. Q. Zhou, R. R. Yang, Q. B. Yang, D. Y. Qing and Q. H. Niu, A novel imidazoline derivative as corrosion inhibitor for P110 carbon steel in hydrochloric acid environment, *Petroleum*, 2015, **1**, 237–243.
12 M. A. Quraishi, D. S. Chauhan and F. A. Ansari, Development of environmentally benign corrosion inhibitors for organic acid environments for oil-gas industry, *J. Mol. Liq.*, 2021, **329**, 115514–115520.
13 Z. Li, X. X. Xu, Y. Li and Z. Y. Liu, Effect of imidazoline inhibitor on stress corrosion cracking of P110 steel in simulated annulus environments of CO_2 injection well, *J. Electroanal. Chem.*, 2021, **886**, 115105–115112.
14 M. M. Solomon, S. A. Umoren, M. A. Quraishi and M. Salman, Myristic acid based imidazoline derivative as effective corrosion inhibitor for steel in 15% HCl medium, *J. Colloid Interface Sci.*, 2019, **551**, 47–60.
15 H. H. Zhang, X. L. Pang, M. Zhou, C. Liu, L. Wei and K. W. Gao, The behavior of pre-corrosion effect on the performance of imidazoline-based inhibitor in 3 wt.% NaCl solution saturated with CO_2, *Appl. Surf. Sci.*, 2015, **356**, 63–72.
16 E. E. El-Katori, M. I. Nessim, M. A. Deyab and K. Shalabi, Electrochemical, XPS and theoretical examination on the corrosion inhibition efficacy of stainless steel via novel

© 2025 The Author(s). Published by the Royal Society of Chemistry

Open Access Article. Published on 28 April 2025. Downloaded on 6/13/2026 3:19:14 AM. This article is licensed under a Creative Commons Attribution-NonCommercial 3.0 Unported Licence.

imidazolium ionic liquids in acidic solution, *J. Mol. Liq.*, 2021, **337**, 116467–116481.

17 H. Li, S. T. Zhang and Y. J. Qiang, Corrosion retardation effect of a green cauliflower extract on copper in H_2SO_4 solution: electrochemical and theoretical exploration, *J. Mol. Liq.*, 2021, **321**, 114450–114462.

18 X. K. He, Y. M. Jiang, C. Li, W. C. Wang, B. L. Hou and L. Y. Wu, Inhibition properties and adsorption behavior of imidazole and 2-phenyl-2-imidazoline on AA5052 in 1.0 M HCl solution, *Corros. Sci.*, 2014, **83**, 124–136.

19 J. Zhang, Z. P. Li, W. M. Zhao, W. Y. Guo and Y. Wang, Theoretical study on corrosion ihibition performance of imidazoline inhibitors, *Acta Pet. Sin., Pet. Process. Sect.*, 2008, **24**, 598–604.

20 H. y. Yang, J. J. Chen, C. N. Cao and D. Z. Cao, Study on corrosion and inhibition on mechanism in H_2S aqueous solutions VII-effect of Imidazoline derivates on the corrosion process of mild steel electrodes in H_2S solutions, *J. Chin. Soc. Corros. Prot.*, 2002, **22**, 321–325.

21 K. G. Zhang, W. Z. Yang, B. Xu, Y. Liu, X. S. Yin and Y. Z. Chen, Corrosion inhibition of mild steel by bromide-substituted imidazoline in hydrochloric acid, *J. Taiwan Inst. Chem. Eng.*, 2015, **57**, 167–174.

22 Y. G. Yan, X. Wang, Y. Zhang, P. Wang, X. H. Gao and J. Zhang, Molecular dynamics simulation of corrosive species diffusion in imidazoline inhibitor films with different alkyl chain length, *Corros. Sci.*, 2013, **73**, 123–129.

23 H. Xu, Q. F. Zhao, J. L. Qin, S. J. Ma and Z. G. Di, Preparation and performance of imidazoline for corrosion inhibitor, *Coating and Protection*, 2021, **42**, 14–18.

24 L. P. Xiong, P. J. Wang, Z. Y. He, Q. Chen and J. B. Pu, Corrosion behaviors of Q235 carbon steel under imidazoline derivatives as corrosion inhibitors: experimental and computational investigations, *Arab. J. Chem.*, 2021, **14**, 102952–103968.

25 A. Singh, K. R. Ansari, M. A. Quraishi and P. Banerjee, Corrosion inhibition and adsorption of imidazolium based ionic liquid over P110 steel surface in 15% HCl under static and dynamic conditions: experimental, surface and theoretical analysis, *J. Mol. Liq.*, 2021, **323**, 114608–114617.

26 A. Singh, K. R. Ansari, Y. H. Lin, M. A. Quraishi, H. Lgaz and I. M. Chung, Corrosion inhibition performance of imidazolidine derivatives for J55 pipeline steel in acidic oilfield formation water: electrochemical, surface and theoretical studies, *J. Mol. Liq.*, 2019, **9**, 341–356.

27 M. Yadav, D. Behera and U. Sharma, Nontoxic corrosion inhibitors for N80 steel in hydrochloric acid, *Arab. J. Chem.*, 2016, **9**, 1487–1495.

28 F. Zhou, H. Wang and Q. Q. Dai, Study on the compound of imidazoline corrosion inhibitor, *IOP Conf. Ser. Earth Environ. Sci.*, 2018, **153**, 52–73.

29 J. D. Olivo, B. Brown and S. Nesic, Modeling of corrosion mechanisms in the presence of quaternary ammonium chloride and imidazoline corrosion inhibitors, *NACE Int Corros Conf Proc.*, 2016, pp. 165–198.

30 Y. Ding, B. Brown, D. Young, S. Nesic and M. Singer, Effect of temperature on adsorption behavior and corrosion inhibition performance of imidazoline-type inhibitor, *NACE Int Corros Conf Proc.*, 2017, pp. 9350–9365.

31 J. D. Olivo, B. Brown and D. Young, Electrochemical model of CO_2 corrosion in the presence of quaternary ammonium corrosion inhibitor model compounds, *NACE Int Corros Conf Proc.*, 2019, pp. 13392–13404.

© 2025 The Author(s). Published by the Royal Society of Chemistry